Astron. Astrophys. 336, L65–L68 (1998)

ASTRONOMY AND ASTROPHYSICS

LETTER

Letter to the Editor

Do solar magnetic elements harbor downflows?

C. Frutiger and S.K. Solanki

Institute of Astronomy, ETH-Zentrum, CH-8092 Zürich, Switzerland

Received 22 June 1998 / Accepted 30 June 1998

Abstract. In a recent paper Bellot Rubio et al. (1997) inverted Zeeman split Stokes profiles to infer the stratification of the temperature, velocity and magnetic field in the photospheric layers of solar magnetic elements (modeled as thin flux tubes). One controversial result of their inversions is the presence of a strong downflow within the flux tubes. In the model underlying their inversion such a downflow is necessary to reproduce the asymmetric shape of the observed V profiles.

We present inversions based on two different flux-tube models, both of which reproduce the Stokes I and V profiles obtained in plages and the network with high accuracy, including the V profile asymmetry. One model is almost identical to that employed by Bellot Rubio et al. (1997), and results in a significant downflow within the flux tube. The other, although similar in most respects, has mass conservation enforced inside the flux tubes, i.e. they contain both an upflow and a downflow which could arise from oscillations or siphon flows. Hence, current data may not be sufficiently sensitive to distinguish between the two velocity structures, so that there is no compelling evidence for a net downflow of matter inside magnetic elements. From a physical point of view the model incorporating mass conservation is to be preferred.

Key words: Sun: magnetic fields – Sun: faculae, plages – polarization – radiative transfer – flux tubes

1. Introduction

The inference of the stratification of thermodynamic and magnetic quantities in the solar photosphere from Zeeman split Stokes profiles has been significantly advanced by an improved inversion technique based on response functions (Ruiz Cobo & del Toro Iniesta 1992, Bellot Rubio et al. 1996). Due to its speed high resolution (polarized) spectra can be used to derive complex atmospheric models with a large set of depth dependent free parameters.

Recently Bellot Rubio et al. (1997, hereafter referred to as BRC) applied this technique to the inversion of Stokes V profiles observed in active region plages. These profiles exhibit a significant asymmetry between their blue and red lobes. Mechanisms based on velocity gradients have been proposed to explain the observed asymmetry (Illing et al. 1975). The common approach is to use a flux tube model whose magnetic field expands with height, so that some lines of sight pass from the magnetic into the non-magnetic atmosphere, which contains a downflow. This approach has been repeatedly demonstrated to reproduce the asymmetry between the areas of the blue and red lobes of the observed V profiles (Grossmann-Doerth et al. 1988; Solanki 1989). On its own such a downflow cannot, however, reproduce the complete V profile shape, in particular not the asymmetry between its blue and red amplitudes. A remarkable result of the inversion carried out by BRC is that a combination of external and internal downflows reproduces the complete asymmetric shapes of the V profiles of the two lines they selected to high accuracy. Since matter cannot flow across field lines in sufficient quantity (Hasan & Schüssler 1985) downflows of several $\mathrm{km\,s^{-1}}$ inside flux tubes, as found by BRC, pose serious problems of mass conservation. Therefore, either another explanation for the Stokes V asymmetry must be found, or our physical notions of solar magnetic elements and the plasma they contain need to be revised. Here we reinvestigate this problem using a new inversion code similar to that of BRC (for a detailed description see Frutiger et al. 1998).

We consider two models which differ in that one allows for either a steady up- or downflow inside the flux-tube (similar to the model of BRC), whereas the other imposes strict mass balance in the sense that we combine two oppositely directed flows of equal mass which can be interpreted as two phases of oscillations within flux tubes. The data we invert are high-resolution Fourier Transform Spectrometer (FTS) measurements (Stenflo et al. 1984) corrected for gravitational redshift, for the Sun-Earth relative motion and for solar rotation (Solanki 1986). In order to facilitate a direct comparison with the results of BRC we restrict ourselves to the two Fe I lines used by them.

2. Models

We have used two sets of models. They have many features in common which we describe first.

The basic structure of the flux-tube model we consider is relatively similar to that employed by BRC. The magnetic field

Send offprint requests to: C. Frutiger

is determined in the thin-tube approximation, i.e. by imposing horizontal pressure balance. The expansion of the field with height is taken into account and line profiles are calculated along 15 vertical rays (we only inverted data obtained close to solar disk center), most of which pass from the magnetic atmosphere (upper layers) into the field-free surroundings (lower layers). The weighted sum over these profiles and the contribution from an additional non-magnetic component, which represents the stray light, constitute the final synthetic profiles. The stray-light component only affects the Stokes I profiles and allows for additional degrees of freedom (temperature, wavelength-shifts) in order to include effects of granular motions in the surrounding quiet sun.

The free parameters of the inversion are as follows: The temperature stratifications in the interior of the magnetic flux tube, $T_{\rm ft}$, and in its non-magnetic surroundings, $T_{\rm nm}$ (14 height points each), as well as the temperature of the stray-light component, $T_{\rm sl}$. The gradient of $T_{\rm sl}(\tau)$ is stratified exactly as in the quiet-sun model of Maltby et al. (1986), but the absolute value at a fixed height is a free parameter. From these temperature stratifications all other thermodynamic quantities like the gas pressure, the electron pressure, or the density are derived assuming hydrostatic equilibrium and LTE (the code of Gustafsson 1973 is used to calculate the opacity, etc). The magnetic field B is determined by B_0, its strength, and α_0, the surface fraction it covers. Both parameters refer to a fixed optical depth τ_0. The stratification follows from the thin-tube approximation. The microturbulence, $v_{\rm mic}$, is assumed to be single valued, since test calculations showed that the observations do not contain sufficient information to deduce the correct $v_{\rm mic}$ stratification. Each spectral line is allowed to be additionally broadened by a macroturbulence, $v_{\rm mac}$, and in case of the stray light component to be shifted in wavelength by an amount δ_λ.

The two models differ mainly in the way flows within the flux tube are dealt with. We therefore discuss the free parameter describing the line-of-sight flow velocity, $v_{\rm los}$, separately for the two models:

Model A *3-component thin flux-tube model*.

The components are: Flux tube (ft), non-magnetic environment (nm) and stray light (sl). The velocities $v_{\rm los,ft}$ and $v_{\rm los,nm}$ are deduced at the same height points as the temperature. The final synthetic Stokes profiles $\boldsymbol{S} = \boldsymbol{S}(\lambda) = [I(\lambda),\, V(\lambda),\, Q(\lambda),\, U(\lambda)]^T$ are a mixture of $\boldsymbol{S}_{\rm pl}$, the contribution from the compound plage component (pl=ft+nm), and the stray light $\boldsymbol{S}_{\rm sl}$:

$$\boldsymbol{S} = (1-\alpha_{\rm sl})\boldsymbol{S}_{\rm pl} + \alpha_{\rm sl}\boldsymbol{S}_{\rm sl}\,.$$

The final free parameter $\alpha_{\rm sl}$ determines the straylight fraction. Model A is similar to the model used by BRC.

Model B *4-component, 2-flux-tubes model*.

Three components of this model correspond to those of model A. To these we add a second magnetic flux-tube component (ft2) that is identical to the first one except for the line-of-sight velocity. This means that we build two plage components (pl1=ft1+nm, pl2=ft2+nm) with the same flux-tube interior (temperature, density, field strength, micro- and macroturbulence, magnetic filling factor) and the same surroundings. The velocity $v_{\rm los,ft2}$ inside the second tube is, however, chosen such that the mass flux at all heights is exactly equal, but with opposite sign, to that in the component ft1, i.e.

$$v_{\rm los,ft2}(z) = -\frac{\alpha_{\rm pl1}}{\alpha_{\rm pl2}}\, v_{\rm los,ft1}(z)\,.$$

Here $\alpha_{{\rm pl}i}$ are weights assigned to the two plage components used to combine their emergent Stokes profiles with the ones from the stray light component:

$$\boldsymbol{S} = \alpha_{\rm pl1}\boldsymbol{S}_{\rm pl1} + \alpha_{\rm pl2}\boldsymbol{S}_{\rm pl2} + \alpha_{\rm sl}\boldsymbol{S}_{\rm sl}\,.$$

Since $\alpha_{\rm pl1}+\alpha_{\rm pl2}+\alpha_{\rm sl}=1$ we chose $\alpha_{\rm pl2}$ and $\alpha_{\rm sl}$ as free parameters.

The idea behind this 4-component model is that due to the limited spatial and temporal resolution of the observations they sample the properties of several unresolved magnetic features. Hence, the up- and downflowing components of the model (i.e. components ft1 and ft2) may represent either the up- and downflowing phases of an oscillation or wave within a flux-tube, or steady up- and downflows in different flux-tubes occurring at the same time (cf. Grossmann-Doerth et al. 1991; Degenhardt & Kneer 1992). In the former case $\alpha_{\rm pl1}$ and $\alpha_{\rm pl2}$ are proportional to the length of the up- and downflowing phases. In the latter case these parameters are proportional to the surface areas covered by the flux tubes harboring the steady down- respectively upflows.

3. Results

The best-fit synthetic profiles from the two models are compared with the spectra observed in an active region plage in Fig. 1. As can be seen from the absolute deviations plotted below each spectrum the 3-component model produces a marginally better fit, but on the whole the two fits are of similar quality. Therefore, we conclude that the two observed lines on their own cannot be used to distinguish between the two models. The quality of the present fits is also similar to that obtained by BRC.

Best fit temperature and velocity stratifications are shown in Fig. 2, along with the standard error estimates (see e.g Press et al. 1992, chapter 15) indicated by error bars plotted at the depths at which free parameters were determined. It should be noted that these estimated errors (and the ones given below) are one-dimensional statistical estimates that do not take into account the coupling between different parameters. Our results, discussed below, demonstrate that the true uncertainties in at least some of the derived parameters can be much larger than the statistical errors.

The results for model A are similar to those presented by BRC, showing a downflow inside and outside of the magnetic flux tube, with both downflow velocities increasing with depth (the decrease with depth of $v_{\rm los}$ in the upper photosphere is not significant, as revealed by the large error bars).

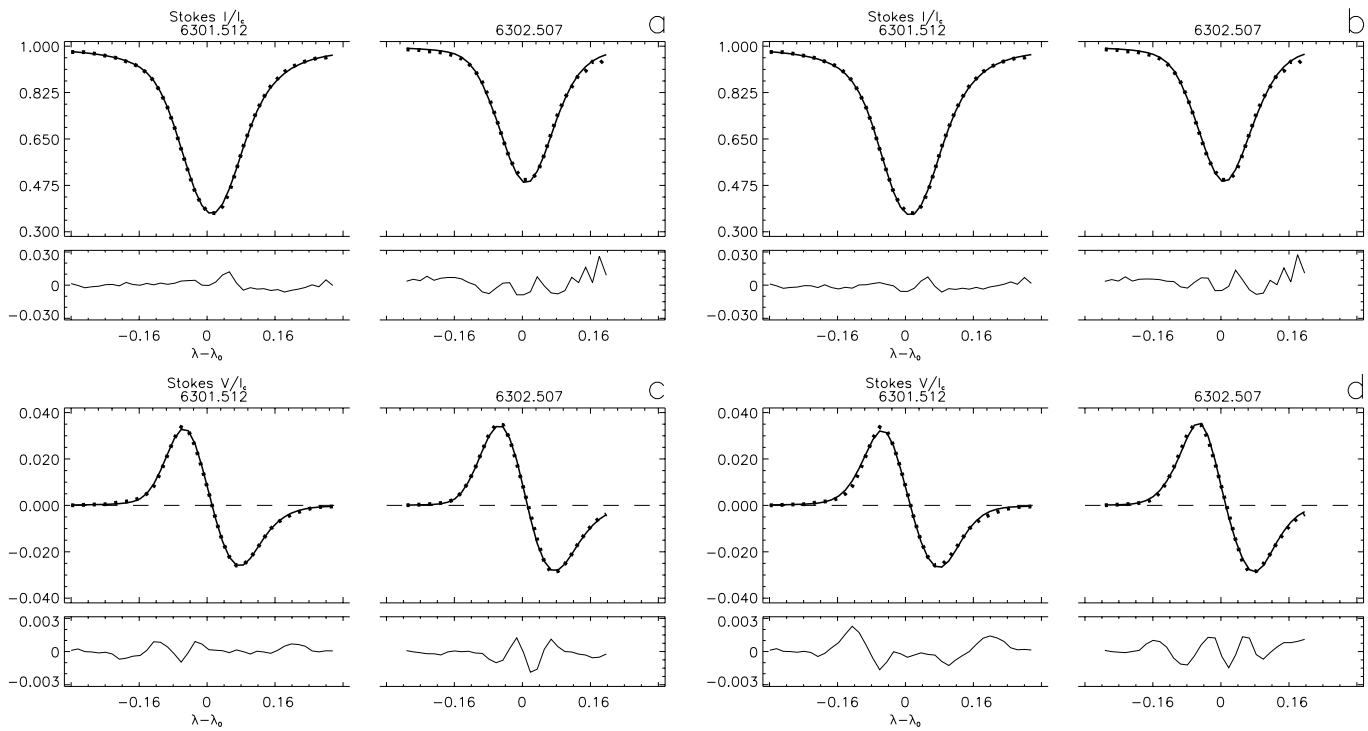

Fig. 1a–d. Observed (dotted) and synthetic (solid) best-fit profiles of the two inverted spectral lines. Stokes I is plotted in the upper panels of Figs. 1a and 1b, Stokes V in Figs. 1c and 1d. The lower panels of each subfigure show the absolute difference between the synthetic and observed profiles. Figs. 1a and 1c refer to model A while Figs. 1b and 1d refer to model B

The best estimates for the depth-independent velocities are $v_{\rm mic,ft} = 0.50 \pm 0.06$ km s^{-1}, $v_{\rm mic,nm} = 0.12 \pm 0.27$ km s^{-1} and $v_{\rm mac} = 1.97 \pm 0.03$ km s^{-1}. We obtained a filling factor $\alpha_0 = 0.152 \pm 0.001$ and a field strength $B_0 = 1533 \pm 9$ G at $\log\ \tau_{\rm ft} = -1$. The contribution from stray light $\alpha_{\rm sl}$ turned out to be 0.189 ± 0.003.

For model B we obtained $v_{\rm mic,ft} = 0.48 \pm 0.09$ km s^{-1}, $v_{\rm mic,nm} = 0.1 \pm 0.38$ km s^{-1}, $v_{\rm mac} = 1.96 \pm 0.03$ km s^{-1}, $\alpha_0 = 0.121 \pm 0.001$ and $B_0 = 1246 \pm 10$ G. The contributions from the different components turned out to be $\alpha_{\rm pl2} = 0.470 \pm 0.004$ and $\alpha_{\rm sl} = 0.187 \pm 0.005$, so that $\alpha_{\rm pl1} = 0.343 \pm 0.009$. Hence, two oppositely directed flows are also able to match both the Stokes V profiles shapes and the zero-crossing wavelength shifts. For our particular data the downflow is about 1.4 times faster than the upflow, and either correspondingly fewer flux tubes harbor such a downflow or it is present for a shorter time within each flux tube.

A fit to the corresponding FTS spectrum of an enhanced network region gave quantitatively similar results and allows the same conclusions to be drawn.

We have searched for additional diagnostics to distinguish between the two models. The addition of 2–3 further spectral lines into the inversion procedure did not bring us closer to this aim. We also used the best fit atmospheres resulting from both models to calculate the Stokes V profile parameters of roughly 230 Fe I lines and 20 Fe II lines in the wavelength range between 5260 Å and 6860 Å, i.e. all unblended Fe lines in the same FTS spectra as the two considered lines. The comparison of their parameters (amplitude asymmetry, area asymmetry and zero crossing wavelength) with the values obtained from the observed FTS spectrum again showed no strong evidence in favor of either model, although there were some specific differences. For example, model A reproduced the line shifts of Fe I lines somewhat better, but was far inferior in reproducing the Fe II lines.

4. Conclusions

We have shown that the inversion of plage and network Stokes profiles driven by minimizing the standard merit function χ^2 strongly depends on the selected model assumptions. Neither of the presented models can be ruled out by the goodness of the fit.

Obviously there is not sufficient information in the data to distinguish between these two types of models directly. However, in model A a large flow across the field lines (> 1 km s^{-1}) is required in order to feed the rapidly increasing downflow with depth, which conflicts with the best physical estimates of such cross-field flows (Hasan & Schüssler 1985). Model B is free of such problems, since mass within the magnetic feature is always conserved. Hence, on physical grounds we favor model B.

Possibly there are even more models that reproduce the observation equally well, e.g. Sánchez Almeida et al. (1996). In any case, current data provide no compelling grounds for a net downflow of matter inside magnetic elements.

Future work must concentrate on increasing the realism of the models but also on finding better diagnostics. There is a

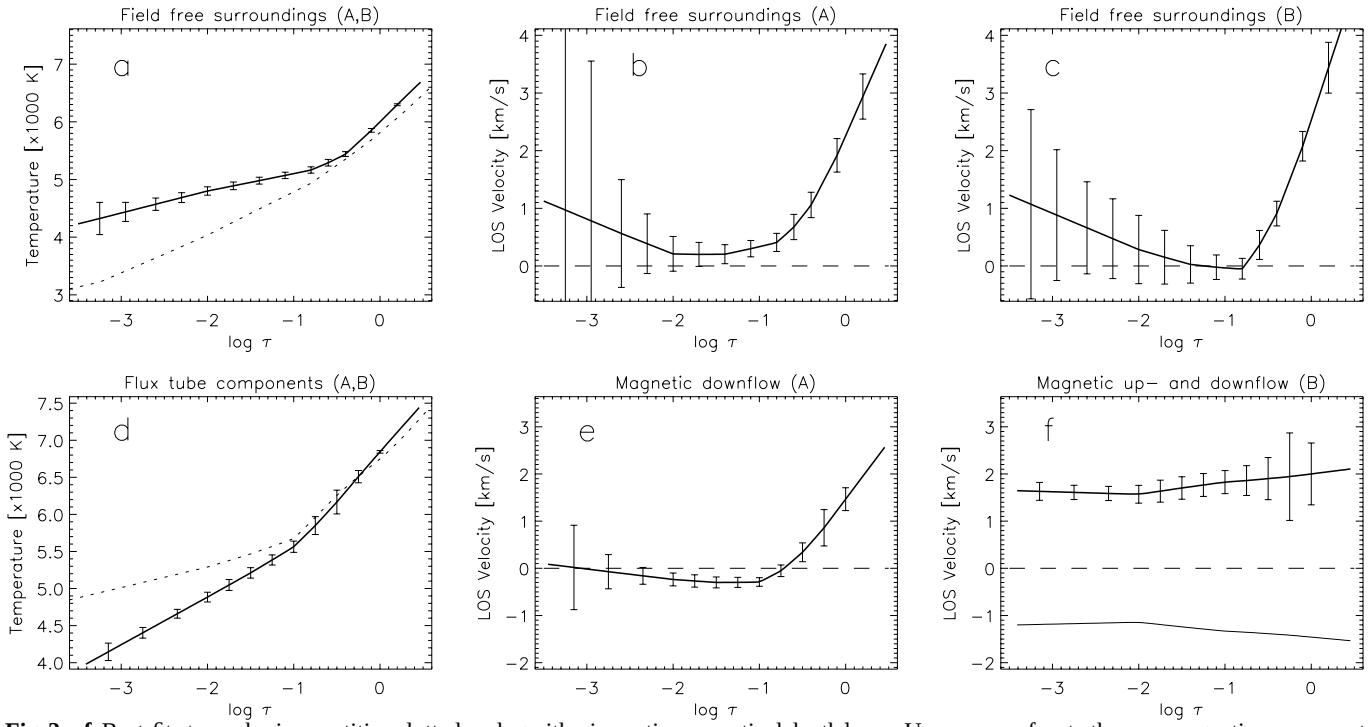

Fig. 2a–f. Best-fit atmospheric quantities plotted vs. logarithmic continuum optical depth $\log\tau$: Upper row refers to the non-magnetic component surrounding the flux tubes, bottom row to the interior of the magnetic flux tubes. The temperature of model A (solid) and model B (dottedd) is plotted in frames a and d. The line-of-sight velocities for model A are given in b and e, while those for model B are plotted in c and f. For a descriptions of models A and B see Sect. 2 of the text

strong need for polarized spectra with higher spatial resolution in order to reveal the nature of solar magnetic velocity fields.

Acknowledgements. We are very grateful to Jo Bruls and Marcel Fligge for contributing to the implementation of response functions in the inversion code used here. This research was supported by the Swiss Nationalfonds under NF grant No. 20-50464.97.

References

Bellot Rubio L.R, Ruiz Cobo B. Collados M., 1996, A&A **306**, 960
Bellot Rubio L.R., Ruiz Cobo B., Collados M., 1997, ApJ **478**, L45 (BRC)
Degenhardt D., Kneer F., 1992, A&A **260**, 411
Illing R.M.E., Landman D.A., Mickey D.L., 1975, A&A **41**, 183
Frutiger C., Solanki, S.K., Bruls J.H.J.M, Fligge M., *in preparation*
Grossmann-Doerth U., Schüssler M., Solanki S.K., 1989, A&A **221**, 338
Grossmann-Doerth U., Schüssler M., Solanki S.K., 1991, A&A **249**, 239
Gustafsson B., 1973, Uppsala Astron. Obs. Ann. **5**, No. 6
Hasan S.S., Schüssler M., 1985, A&A **151**, 69
Maltby P., Avrett E.H., Carlsson M., Kjeldseth-Moe O., Kurucz R.L., Loeser R., 1986, ApJ **306**, 284
Press W.H., Flannery B.P., Teukolsky S.A., Vetterling W.T., 1990, Numerical Recipes. The Art of Scientific Computing, Cambridge University Press, Cambridge
Ruiz Cobo B., Del Toro Iniesta J.C., 1992, ApJ **398**, 375
Sánchez Almeida J., Landi Degl'Innocenti E., Martínez Pillet V., Lites B.W., 1996, ApJ **466**, 537
Solanki S.K., 1986, A&A **168**, 311
Solanki S.K., 1987, Ph.D. Thesis No. 8309, ETH, Zürich
Steiner O., Grossmann-Doerth U., Knölker M., Schüssler M., 1996, Solar Phys. **164**, 223
Stenflo J.O., Harvey J.W., Brault J.W., Solanki S.K., 1984, A&A **131**, 333